Cellulose in New Metal-Complexing Solvents. 2. Semidilute Behavior in Cd-tren

Kay Saalwächter and Walther Burchard*

Institute of Macromolecular Chemistry, Albert-Ludwigs University of Freiburg, 79104 Freiburg, Germany

Received September 15, 2000; Revised Manuscript Received May 11, 2001

ABSTRACT: A high molar mass cotton linters cellulose was investigated by static and dynamic light scattering in semidilute solutions of the cadmium complexing Cd-tren (tren = tris(2-aminoethyl)amine). In this solvent cellulose has a Kuhn segment length of 15.3 nm and represents a semiflexible chain. Apparent molar masses $M_{app}(c)$ and apparent radii of gyration $R_{g,app}(c)$ were measured by light scattering. The influence of interchain interactions could be split off using either the theoretically well-known interaction among flexible chains or thin rigid rods, respectively. Estimations of the true molar mass $M_w(c)$ and true radius of gyration $R_g(c)$ at finite concentration c were obtained. Both molecular parameters increased with concentration when the overlap concentration was exceeded by a factor 4. Simultaneously, a slow mode of motion appeared in dynamic light scattering. The observations were interpreted as a result of association. The thermodynamic interaction could also be separated from the mutual diffusion coefficients and yielded the self-diffusion coefficients. A hydrodynamic radius $R_h(c)$ was defined by applying the Stokes−Einstein relationship to the self-diffusion coefficient. This radius is interpreted as a correlation length for the influence of hydrodynamic friction. The zero shear viscosity showed behavior common to other linear chain molecules in solution. Shear thinning occurred in the semidilute regime. The curves could be fitted by the Cross approximation. A scaled master curve was obtained. The relaxation times for disengagement τ_d increased with a power of 3.6 as the concentration was increased. This exponent is larger than 2.0 as predicted from the reptation model. The reversibly associating bonds cause a significant disengagement retardation of entangled chains.

Introduction

Cellulose is a semicrystalline fibrous material in which the individual chains are highly stabilized by a well-organized system of hydrogen bonds.[1,2] These hydrogen bonds regularly interconnect the various chains. They are also present between neighbored monomer units, the β(1,4)-linked anhydroglucose units (AGU), and cause a pronounced stiffening of the chains. This network of hydrogen bonds is the main reason for the poor solubility. Uncommon solvents have to be used for breaking, at least the interchain hydrogen bonds. All solvents currently used for cellulose form clear, though often colored, solutions. Detailed studies of the solution properties revealed, however, that the material is often not completely dissolved to the level of individual chains.[3]

Recently, two new water-containing metal complexes were developed which coordinatively bind to the deprotonated OH groups in the C2 and C3 position of the AGU.[4,5] These solvents were designed such that only two of the coordination sites remained free for the binding to the deprotonated polyol of cellulose. In a short-hand writing the solvents were denominated as Ni-tren and Cd-tren, respectively. Four of the six coordination sites of the Ni^{2+} and Cd^{2+} cations are bound to the tetradentic ligand tris(2-aminoethyl)amine $N[-CH_2-CH_2-NH_2]_3(OH)_2$ (= tren), leaving two sites in the cis configuration free for the mentioned binding to the AGU. The structure of the Cd complex in the free and coordinatively bound states is shown in Figure 1. The coordinative binding destroys the native network of hydrogen bonds and helps ripping the crystalline structure of cellulose by the bulky tren ligand. Ni-tren was found to form the more stable complex than Cd-tren but is deep blue. Cd-tren, on the other hand, is only weakly yellowish and proved to be more suited for light scattering measurements.

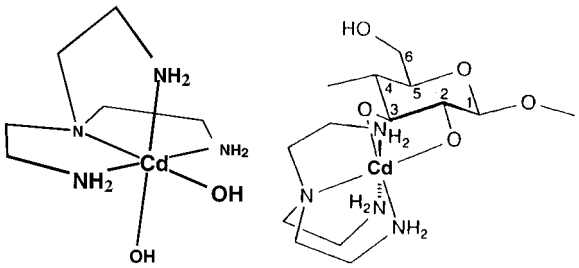

Figure 1. Chemical structure of the Cd-tren complex in its free form and bound stage to the cellulose chains. tren is the tetradentic ligand tris(2-aminoethanol)amine.

The coordinative binding of a metal complex to a polymeric chain is a striking specialty in polymer science. Uncommon solution behavior could be expected. In a previous study[6] we carried out a rather comprehensive characterization of cellulose in dilute solutions of Cuoxam, Ni-tren, and Cd-tren. We obtained molecular dispersity and common solution behavior. A remarkable chain stiffness was found that could be explained by an enhanced strength of *intra*chain hydrogen bonding.[7]

In thermodynamic equilibrium the composition of the complex and the free compounds is expected to change when the concentration of ligands is increased. In the present study we extended the range of cellulose concentrations considerably beyond the overlap concentration and examined whether uncommon effects would be observed. Cd-tren was used as solvent. The applied concentration ranged from $c = 0.1$ mg/mL to $c = 18$ mg/mL (1.8% w/v) which corresponds to $c = 54c^*$, where c^* is the overlap concentration. A limit of solubility is reached when the molar concentration of anhydroglu-

10.1021/ma0016073 CCC: $20.00
Published on Web 06/28/2001

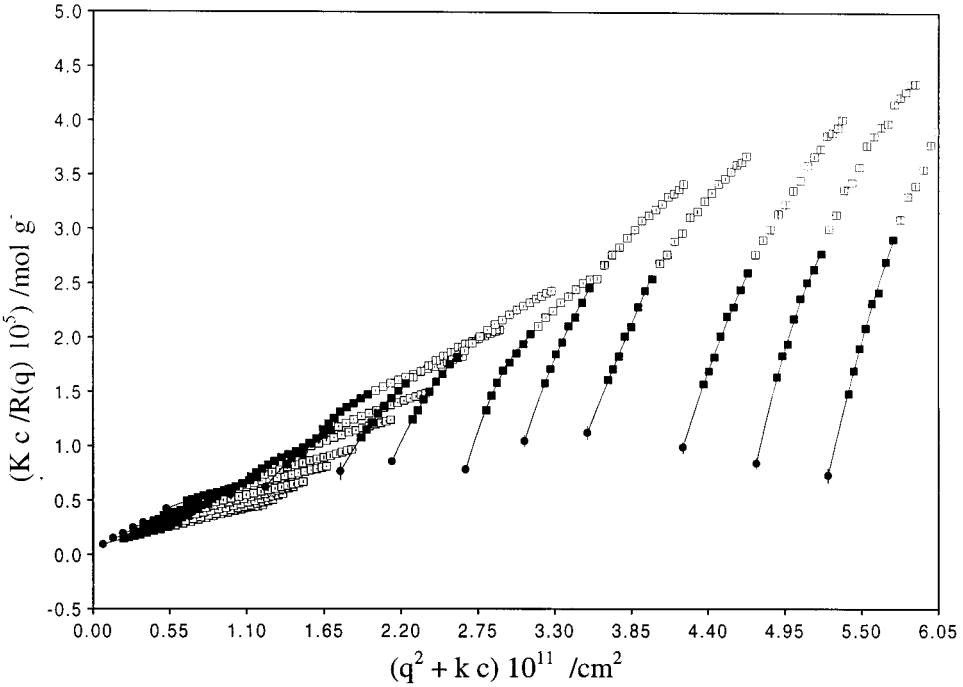

Figure 2. Zimm plot from a cotton linters cellulose in Cd-tren. The concentration ranged from $c = 0.5$ to 15.3 mg/mL; the latter corresponds to $c = 43.5c^*$ where $c^* = (A_2M_w)^{-1} = 0.352$ mg/mL is the overlap concentration. $M_w = 2.22 \times 10^6$ g/mol, $R_g = 145$ nm, and $A_2 = 1.25 \times 10^{-3}$ mL/g^2. For the determination of the initial slopes in the angular dependencies only the data of the filled squares ($\theta = 30$ to 65°) were used, and the extrapolation was made by a quadratic fit. The filled circles represent the data for each concentration at $\theta = 0°$ and include also the limiting curve at $c = 0$ (data outmost to the left).

cose units exceeds that of the Cd-tren complex. This happens at a concentration of about $c = 130$ mg/mL (13% w/v) of cellulose, a region that is still far away from the highest applied concentration.

The properties of semidilute solutions from flexible linear chains have been measured in a large number of laboratories and were found to be in an excellent agreement with the scaling predictions by de Gennes[8] and, more recently, with the renormalization group (RG) theory.[9] Also, stiff chain molecules from bacterial polysaccharides were studied but were found to follow a different universality class.[10,11] Cellulose is a semiflexible chain molecule with a Kuhn segment length of $l_K = 15.3 \pm 0.3$ nm in Cd-tren[6] that is about 8 times larger than found for polystyrene. It appeared of interest whether the coordinative binding exerts a special influence on the structure of cellulose at concentrated solutions in that solvent.

In the following we report results from static and dynamic light scattering and rheological measurements. The interpretation of the data was faced with a number of facts which are not encountered in dilute solutions. These are in short a peculiar, strong angular dependence of scattered light, an unusual concentration dependence, and the appearance of a slow motion in dynamic light scattering. Notably, these phenomena occurred simultaneously when a certain concentration was exceeded. This observation gave evidence for association. In contrast to semidilute solutions of linear, nonassociating chains there exists presently no well-established theory for associating systems which could be applied to experimental data. In an attempt of quantitative description we started with well-known approximations for dilute solutions and nonassociating systems in the semidilute regime. Tentatively we then extended these initial stages to include association. Attempts of other authors will be mentioned in due course. Because of the unaccustomed fragments of theory, the paper is organized in a somewhat different manner than commonly used. Instead of presenting separately theoretical relationships, we found it more convenient in the present case to recall relationships of current theories when they are needed for interpreting the experimental results. The results are partially discussed in the corresponding sections. A comprehensive discussion is given at the end of the paper.

Experimental Section

Sample. A high molar mass cotton linters (Lin3) with degree of polymerization $DP_w = 9350$ and radius of gyration $R_g = 145$ nm was used. It was the only sample from the series studied in part 1[6] that was sufficiently large for the present type of investigation.

Solvent. Cd-tren was used as solvent. Its preparation and clarification for light scattering measurements were described in part 1.[6]

Instruments. All instruments were the same as previously described.[6] The wavelengths of the light were $\lambda_0 = 632.8$ nm (HeNe laser) for the static LS and $\lambda_0 = 648.2$ nm (Kr ion laser) for the dynamic LS instrument.

Results

Static Light Scattering. Static light scattering data are mostly plotted in the form of a Zimm diagram. Figure 2 shows such a Zimm plot from a linters cellulose in Cd-tren. A concentration range from 0.5 to 15.3 mg/mL was covered. The clarification required a special treatment that was described in detail in paper 1.[6] Compared to Zimm plots from common synthetic polymers in dilute solution, this diagram exhibits unusual behavior. The uncommon properties occur beyond a concentration of 2 mg/mL. In the dilute regime quite normal behavior was found.[6] Good reproducibility was obtained also for the high concentrations, well above the overlap concentration. Both the q^2 and concentration

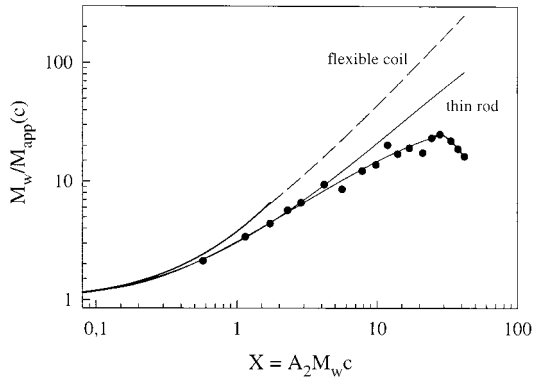

Figure 3. Reduced osmotic modulus $M_w/M_{app}(c) = (M_w/RT)(\partial\pi/\partial c)$ as a function of the scaled concentration $X = A_2M_wc$. The apparent molar mass is obtained from the forward scattering (at scattering angle $\theta = 0$) as $M_{app}(c) = R_{\theta=0}(c)/Kc$. Symbols: experimental data; dashed and full lines: theoretical curves for flexible coils and rigid rods.

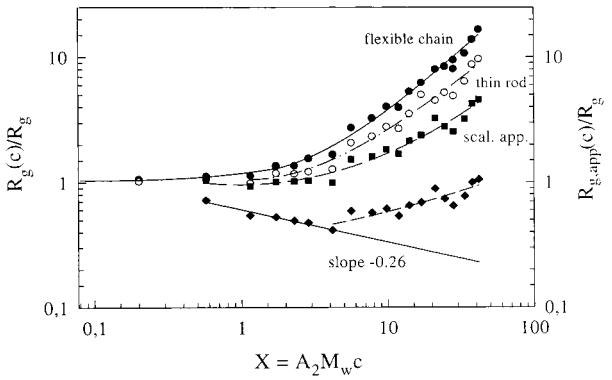

Figure 4. Normalized apparent radius of gyration $R_{g,app}(c)/R_g$ as a function of the scaled concentration X (◆). Calculated true radii of gyration $R_g(c)/R_g$, on the basis of eq 15 for interactions among flexible coils (●) and thin rods (○), respectively. The solid line of slope −0.26 is a fit to the first six points of $R_{g,app}(c)/R_g$; the squares and the curve labeled as scal.app. correspond to the ratio of measured apparent radii to that predicted by the solid line.

dependencies were linear and allowed extrapolation toward zero concentration without difficulties, where

$$q = (4n_0\pi/\lambda_0)\sin(\theta/2) \tag{1}$$

with n_0 the refractive index of the solvent, λ_0 the wavelength of the used light in a vacuum, and θ the scattering angle. This gave the three relevant molecular parameters $M_w = 2.22 \times 10^6$ g/mol, $R_g = 145$ nm, and $A_2 = 1.25 \times 10^{-3}$ mL/g^2.[6] At concentrations larger than 2 mg/mL two new effects appeared: (i) at small angles a down-turn started to develop and gained increasingly more influence at higher concentrations; (ii) the extrapolated data of Kc/R_θ toward $\theta = 0$ no longer increased linearly with concentration but bent down and eventually decreased again.

In the present paper we confined ourselves to a discussion of the initial part of the angular dependencies. Because of the curvature, only the data points from angles up to 65° were used for extrapolation to zero scattering angle, which made possible an unproblematic description by a quadratic fit. The interpretation of the whole angular dependence will be matter of concern in a forthcoming paper.

In the following apparent molar masses and apparent radii of gyration are introduced as follows:

$$\left[\frac{Kc}{R_{\theta=0}}\right]_c \equiv \frac{1}{M_{app}(c)} \tag{2}$$

$$\left[3\,\frac{\text{slope}}{\text{intercept}}\right]^{1/2} = [3(\text{slope} \times M_{app}(c))]^{1/2} \equiv R_{g,app}(c) \tag{3}$$

Both are evidently functions of the concentration. They will be evaluated separately. Figure 3 shows the concentration dependence of the reciprocal apparent molar mass normalized by the weight-average molar mass at zero concentration, $M_w/M_{app}(c)$. Instead of the actual concentration c, a scaled concentration $c/c^* \equiv X$ was chosen, where the overlap concentration c^* is defined here via the osmotic virial coefficient A_2 as

$$c^* \equiv (A_2M_w)^{-1} = 0.36 \text{ mg/mL} \tag{4}$$

Figure 3 contains also theoretical dependencies for flexible chains[12] and for infinitely thin rods.[13] The experimental data follow for small X values the curve of a rod but show deviation to smaller values at large X.

Figure 4 represents the results for the apparent radius of gyration $R_{app}(c)/R_g$, normalized by the radius of gyration R_g at zero concentration as a function of the scaled concentration X. The experimental data first decrease with concentration but change to an increase beyond the overlap concentration, i.e., at $X > 4$. The straight line of slope $q_R = -0.26$ is a linear fit through the first six points of $R_{app}(c)$, which will be discussed below together with the other curves in Figure 4.

Dynamic Light Scattering. In dynamic LS a time correlation function (TCF) of the scattering intensity is measured which is defined as the average product of a scattering intensity $i(0)$ at time $t = 0$ and $i(t)$ at a short time later. This intensity TCF decays exponentially, but often as a non-single-exponential, with the delay time toward a baseline that corresponds to the square of static LS. For convenience, this TCF is normalized by the baseline and is denoted as $g_2(t,q) \equiv \langle i(0)\, i(t)\rangle/\langle i(\infty)\rangle^2$, which now decays from a value somewhat below 2.0 toward 1.0 (baseline) as the delay time is increased. The decay time is related to the mutual diffusion coefficient $D(c)$ but can also be influenced by internal modes of motion. Because of these internal motions and also for polydisperse samples, deviations from a single-exponential behavior are obtained. In these cases the TCF is usually described by a cumulant fit that is defined as[14]

$$\ln(g_2(t,q)) = -\Gamma(q,c)t + \Gamma_2(q,c)t^2 - \Gamma_3(q,c)t^3 + \ldots \tag{5}$$

where $q = (4\pi n_0/\lambda)\sin(\theta/2)$ with n_0 the refractive index of the solvent and λ the wavelength in the solution; the various Γ_i are called first and higher cumulants. The following treatment is based on three cumulant fits, but the interpretation is confined to the first cumulant that is related to an apparent, angular dependent mutual diffusion coefficient $D_{app}(q,c)$. For sufficiently small values of qR_g it can be described by the equation[15]

$$\frac{\Gamma}{q^2} = D_{app}(q,c) = D_c(1 + CR_g{}^2q^2 - \ldots) \tag{6}$$

in which D_c is the concentration-dependent mutual

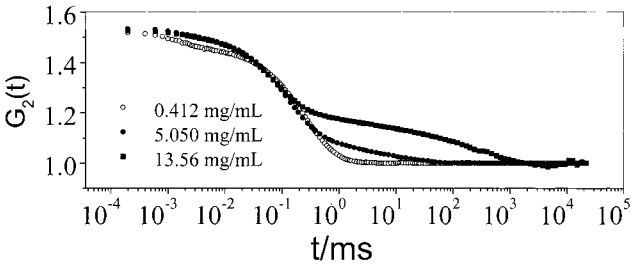

Figure 5. Time correlation functions from some concentrations at 90°. The diffusion coefficients of the fast and slow motions and their amplitudes were determined by the Kohlrausch−Williams−Watts procedure.

diffusion coefficient. The coefficient C contains the slowest internal relaxation mode but will not be considered here in detail. Accordingly, the mutual diffusion coefficient is obtained after extrapolating the apparent diffusion coefficient to zero scattering angle. In the limit of zero concentrations the translational diffusion coefficient D_z is obtained. It is related to a hydrodynamic effective radius R_h via the Stokes−Einstein relationship

$$R_h = \frac{kT}{6\pi\eta_0 D_z} \tag{7}$$

Figure 5 shows time correlation functions of cellulose in Cd-tren at various concentrations. At low concentrations only one mode of motion is observed, but when the overlap concentration is exceeded, a second slower motion occurs that is strongly slowed at further increase of concentration. Such bimodal curves are difficult to describe by a cumulant fit. In such cases two other techniques can be applied. The one consists of the use of the CONTIN inversion program developed by Provencher[16] and the other in a fit of the TCFs by means of Kohlrausch−Williams−Watts (KWW) stretched exponential functions.[17] We always applied all three techniques, i.e., (i) the cumulant fit, (ii) the CONTIN inversion, and (iii) the KWW fit. A critical consideration of the advantages and disadvantages with three techniques is given in the Appendix.[18−22] However, in the present case most reliable results were obtained with the KWW procedure. The first cumulant remained of interest because it represents the z-average of the translational diffusion coefficient. In the dilute regime only one relaxation process was found, but in the semidilute regime another slow diffusive mode appeared. In these cases the first cumulant (or the z-average diffusion coefficient) was calculated from the sum of the two diffusion coefficients weighted by their amplitudes (frequency of occurrence). The result is shown in Figure 6, and the actual data are given in Table 2 that also contains the amplitude factors for the fast and slow motions. For details see the discussion to eqs 17 and 18.

Rheology. *Zero Shear Viscosity.* In the dilute regime the specific viscosity of the sample was measured in a capillary Ubbelohde viscometer as a function of concentration with the highest concentration that corresponded to $c[\eta] = 1.76$, where $[\eta] = 1573$ mL/g is the intrinsic viscosity of the sample. For the concentrations in the semidilute regime measurements were made in a cone−plate geometry of a CS Bohlin rheometer at different shear rates $d\gamma/dt$, and the viscosities were then extrapolated to $d\gamma/dt = 0$. The result is plotted in Figure 7 in a double-logarithmic scale. A fairly weak increase

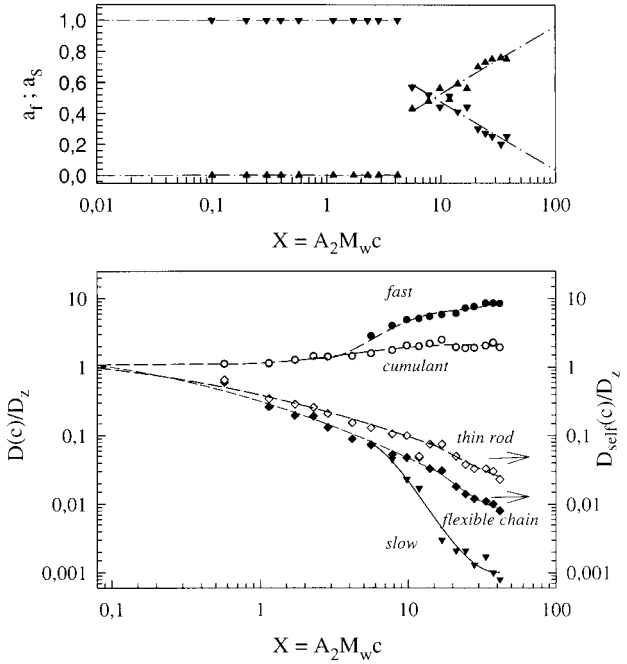

Figure 6. Concentration dependence of the fast and slow diffusion coefficients and of the mutual diffuison coefficient $D(c)/D_z$. In the dilute regime $D(c)$ could be determined from the first cumulant. At higher concentrations the cumulant fit is inaccurate and was replaced by the weighted sum of the fast and slow diffusion coefficients ($D(c) = a_f D_f(c) + a_s D_s(c)$). The upper part of the figure shows the amplitudes of the two components. The figure also shows the concentration dependence of the normalized self-diffusion coefficient obtained after splitting off the thermodynamic interaction among flexible coils (●) and rigid rods (○), respectively (see eq 20).

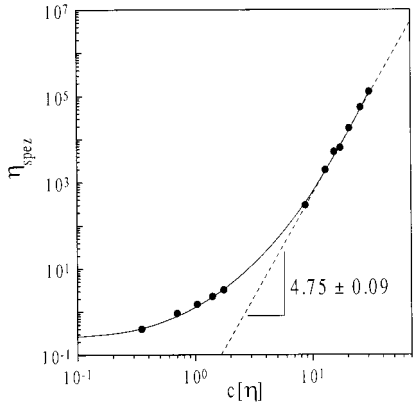

Figure 7. Zero shear viscosity as a function of $c[\eta]$, where $[\eta]$ is the intrinsic viscosity of the sample.

of the zero shear viscosity is found in the dilute concentration regime that changes into a steep increase when a value of $c[\eta] = 4$ is exceeded. In that regime the curve approaches power law behavior with an exponent of $\mu = 4.75 \pm 0.09$. An intersection point of the two regimes can be extrapolated which corresponds to $c[\eta] = 4$ and $\eta_{spec,cr} \cong 10$.

Shear Rate Dependence of the Solution Viscosity. Macromolecules in solution often show shear thinning of the solution. In the dilute regime no shear dependence was observed. The lowest concentration at which a shear thinning could be observed with the Bohlin constant stress rheometer was $c = 5$ g/L, corresponding to a value of $c[\eta] = 8.75$. For higher concentrations the effect of shear thinning became more and more pronounced. Figure 8a shows the result of η/η_0 as a function of the

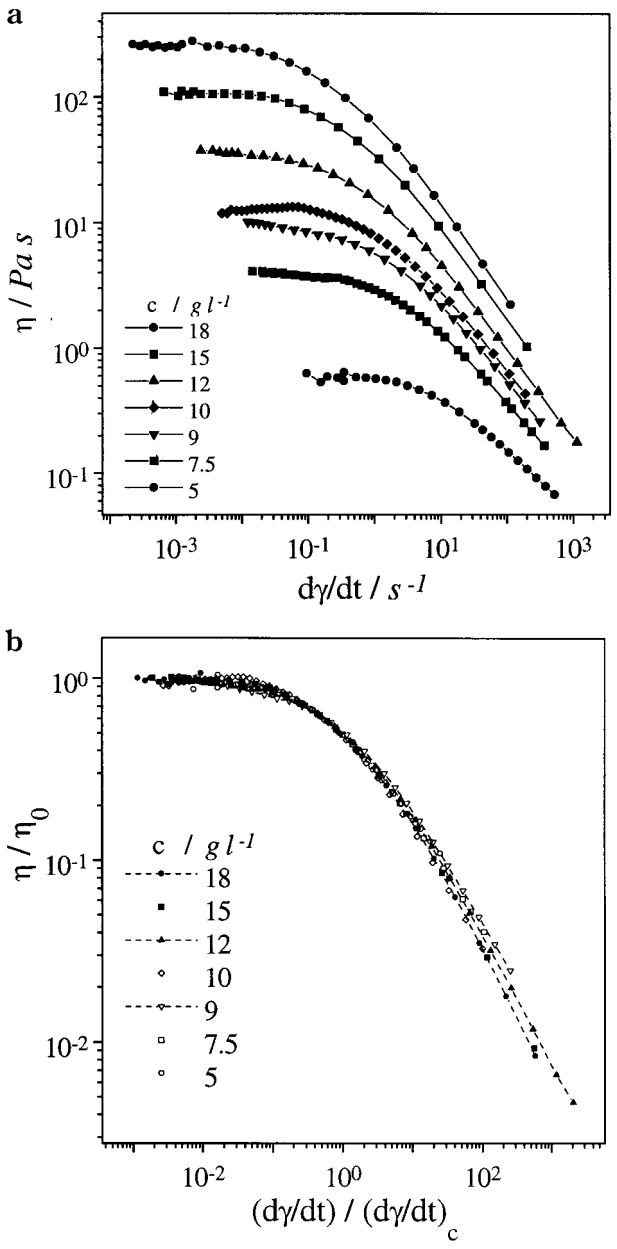

Figure 8. (a) Shear gradient dependence of viscosity from seven different concentrations. (b) Scaling after applying the Cross approximation of eq 22.

shear gradient dγ/dt in a double-logarithmic plot for seven concentrations (5−18 g/L). All curves approach a constant value at low shear gradients that indicates Newtonian behavior. At large shear gradients the curves approach approximately the same asymptotic slope of a power law.

Discussion

Figures 3, 4, and 6 clearly demonstrate marked changes in behavior when the overlap concentration is exceeded approximately by a factor 4 (i.e., $X = 4$). To a certain extent a change in behavior was expected, because at $c \gg c^*$ entanglement of the chains should become effective that eventually leads to a transitional network. In common entangled systems the points of entanglement are not fixed, and the chains can still move through slip-links. No increase in molar mass and dimension should be observable. The drastic increase of the apparent radius of gyration, the onset of a slow motion (that increases in amount and is markedly slowed with concentration), and the turnover in the normalized apparent molar mass are clear indications for the formation of large clusters which are held together by physical bonds. The question arises whether these association phenomena can be quantified. We were interested to know what the true particle weight and size would be at concentration c and also to get some ideas on the shape of the particles. The measured apparent molar mass and radius of gyration are highly influenced by repulsive interactions which are exerting a strong effect. In the following we show that these interactions can be split off. To this end current theories have to be consulted. We will do this for the apparent molar mass, the apparent radius of gyration, and the mutual diffusion coefficient.

Osmotic Modulus. According to statistical thermodynamics, the forward scattering, i.e., the extrapolated scattering intensity at scattering angle $\theta = 0$, is related to the osmotic compressibility $RT(\partial c/\partial \pi)_{P,T}$ as given by[23]

$$R_{\theta=0} = KcRT\left(\frac{\partial c}{\partial \pi}\right)_{P,T} \tag{8}$$

Expansion of the osmotic pressure in a virial series gives the well-known relationship

$$\frac{Kc}{R_{\theta=0}} = \frac{1}{M_w}[1 + 2A_2M_wc + 3A_3M_wc^2 + ...] \equiv \frac{1}{M_{app}(c)} \tag{9}$$

or

$$\frac{M_w}{M_{app}(c)} = \frac{M_w}{RT}\left(\frac{\partial c}{\partial \pi}\right)_{P,T} = [1 + 2A_2M_wc + 3A_3M_wc^2 + ...] \tag{9'}$$

For convenience the ratio of the true to apparent molar mass will be called the reduced osmotic modulus. It describes the force that is needed to bring particles closer together against the repulsive potential of the particles. This scaled osmotic modulus has no dimensions, and therefore, also the right side must be a dimensionless quantity. For flexible linear chain molecules des Cloizeaux[24] and later de Gennes[8] made the assumption that the osmotic pressure and thus also the osmotic modulus are universal functions of $c/c^* = A_2M_wc \equiv X$. Such behavior was known for long for hard spheres,[25] but it was realized to hold also for stiff chain molecules[11] and various types of branched macromolecules.[26] Universal means here that the same curve is obtained for a special type of polymer when the concentration is changed or the molar mass. However, each architecture has its own master curve. This allows us to rewrite eq 9′ as follows:

$$\frac{M_w}{M_{app(c)}} = [1 + 2X + 3g_aX^2 + 4h_aX^3 + ...] = f(X,\text{architecture}) \tag{10}$$

In this equation the coefficients g_a and h_a are structure-dependent and should represent the relation of the third and fourth virial coefficients to the second virial coefficient. In previous papers we noticed that eq 10 gives

the correct value for the third virial coefficient as long as the overlap concentration is not too strongly exceeded. In the higher concentrated regime more than four virial coefficients are effective. However, the virial coefficients assume positive and negative values, and each individual virial coefficient starts to diverge. Thus, eq 10 has to be considered as an empirical fit function. Asymptotic behavior can be described by a scaling assumption together with the condition that the osmotic modulus should become independent of the molar mass. In a previous paper[27] we showed that the fit curves approach this asymptote is given by the exponent $p = 1/(3\nu - 1)$ and describes correctly the crossover from virial to scaling behavior. The exponent ν describes the power law behavior of R_g as a function of M_w and is related via $\nu = 1/d_f$ to the fractal dimension of the particles. Analytical relationships have been derived for hard spheres,[25] flexible chains,[12] and stiff cylinders[13] of various axial ratios. The latter expression becomes insensitive to the cross-sectional diameter when the axial ratio $p_{cross} = L/d > 100$, and only the contribution of the second virial coefficient remains effective.

The measured curve follows at low concentration the behavior of thin stiff rods. The stiff rod behavior is somewhat unexpected, but similar results were obtained previously with other very stiff bacterial polysaccharide chains.[10] We consider the fit curve of the reduced osmotic modulus for stiff rods as a *master curve* that should be obeyed as long as no structural changes occur in the semidilute regime. The cellulose of consideration consists of about 300 Kuhn segments and should already fulfill the condition of perturbed Gaussian chains. For this reason also the theoretical curve for the osmotic modulus of flexible chains, as derived by Ohta and Oono,[12] will be taken as a reference. The corresponding master curves for Gaussian chains and for the stiff rod are given by eq 11 (ref 12) and eq 12 (ref 13), respectively

$$\left(\frac{M_w}{RT}\frac{\partial\pi}{\partial c}\right)_{\text{flex chain}} = 1 + \frac{1}{8}\left[9\bar{X} - 2 + \frac{2}{\bar{X}^2}\ln(1+\bar{X})\right] \times \exp\left[\frac{1}{4}\left(\frac{1}{\bar{X}} + \left(1 + \frac{1}{\bar{X}^2}\right)\ln(1+\bar{X})\right]\right. \quad (11)$$

$$\bar{X} = \frac{16}{9}X = \frac{16}{9}A_2M_wc$$

$$\left(\frac{M_w}{RT}\frac{\partial\pi}{\partial c}\right)_{\text{stiff rod}} = \frac{1 + 2(1+1/p)\hat{X} + 2/p)\hat{X}^2}{(1-\hat{X}/p)^4} \quad (12)$$

$$\hat{X} = X(1+3/p) = A_2M_wc(1+3/p)$$

The experimental points start to deviate toward smaller values of $M_w/M_{app}(c)$ at about $X = 4$. Such behavior can be taken as the onset of association, a supposition that was confirmed by the evaluation of the dimensions (to be shown in the next section).

The assumption of association requires a modification in eqs 9 and 9′. Now the weight-average molar mass has to be replaced by $M_w(c)$ that takes into account the increase of the molar mass at concentration c as a result of cluster formation. In the following an approximate procedure is suggested for determining the molar mass at the finite concentration. For each concentration the ratio of the measured osmotic modulus to that of the master curve is formed:

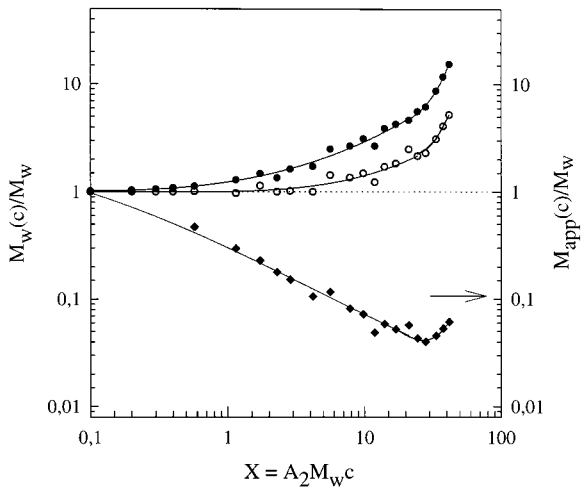

Figure 9. Concentration dependence of the normalized apparent molar mass $M_{app}(c)/M_w$ and of the true molar masses $M_w(c)/M_w$ derived from $M_{app}(c)$ after correction for thermodynamic interaction among coils (●) and rods (○), respectively.

$$\frac{[\partial\pi/\partial c]_{\text{experiment}}}{[\partial\pi/\partial c]_{\text{master curve}}} = \frac{M_w(c)}{M_w}\frac{1 + 2A_2M_wc + 3A_3M_wc^2 + ...}{1 + 2A_2M_w(c)c + 3A_3M_w(c)c^2 + ...} \cong \frac{M_w(c)}{M_w} \quad (13)$$

No significant change in the repulsion is assumed when association takes place which gives the right-hand expression in eq 13. Figure 9 shows the increase of $M_w(c)/M_w$ using the master curves of osmotic moduli for rods and flexible chains, respectively.

The equation for the reduced osmotic modulus is not fully correct for chains with associating stickers, because the interaction is reduced by the formation of associative bonds. In all theories,[28−32] this part of attractive interaction is proportional to the concentration with an amplitude factor of λ/l_S^2 where λ represents the strength of attractive interaction and l_S is the length between two stickers along the chain. Therefore, this attractive part can be incorporated in the second virial coefficient that is now somewhat smaller than for the chain without stickers. This fact would reduce the second viral coefficient of the aggregates and would lead to a somewhat smaller value for the molar mass $M_w(c)$. On the other hand, this molar mass increases with concentration and causes an increase of the denominator. The magnitudes of these two effects could not be estimated with the measured data, but both effects may largely compensate each other.

Radius of Gyration at Finite Concentration. The radius of gyration at infinite dilution can be determined from the angular dependence of the scattered light using eq 3 without knowing the actual molar mass and the architecture of the dissolved particles. At finite concentration the radius determined by eq 3 is strongly influenced by the repulsive volume interaction, and only an apparent radius of gyration is found. However, when the Debye expansion for the scattered light at finite concentration is used, one obtains a relationship between the apparent and the true radius of gyration that

is given by

$$\frac{1}{M_{app}(c)}\left[1+\frac{1}{3}q^2R_{app}{}^2(c)\right] = \frac{1}{M_w(c)}\left[1+\frac{1}{3}q^2R_g{}^2+2A_2M_w(c)c+3A_3M_w(c)c^2\right] \quad (14)$$

from which one finds

$$R_g(c) = R_{app}(c)\left(\frac{M_w(c)}{M_{app}(c)}\right)^{0.5} \quad (15)$$

Figure 4 shows the concentration dependence of the true radii of gyration. Compared to the decreasing apparent radius of gyration, the true radius of the macromolecules remains constant up to $c = 4c^*$ if rodlike behavior is assumed, and it increases weakly when flexible chain behavior is assumed. At larger values a strong increase of the radii occurs that clearly indicates association.

The virial approach is certainly correct as long as no coil−coil interpenetration occurs. This is the case for hard spheres but will remain a good approximation also for highly branched structures where only the outer chains can interpenetrate. However, the quality of this approximation is not obvious if a deep interpenetration becomes possible, as was found for flexible linear chains. Here a scaling approach has been successful,[8] in which an asymptotic decrease of the apparent radii of gyration is predicted with an exponent $q_{scal} = -(\nu - \nu_0)/(3\nu + 1)$. Using the data from the renormalization group theory,[9] the exponent becomes $q_{scal} = -0.115$. We fitted the decrease of $R_{app}(c)$ by a power law and found $q_R = -0.26$, a value that is more than 2 times larger in value as predicted by theory. If the experimental value of $\nu = 0.595 \pm 0.035$ is used,[6] no significant change with $q_{cal,exp} = -0.12 \pm 0.05$ is obtained. The disagreement between theory and experiment may be a result of the chain stiffness that reduces the long chain to a segment number of 300, and this number might be not sufficiently large to guarantee asymptotic behavior that is required for scaling relationships.

Disregarding this failure of scaling behavior, we pragmatically determined the ratio of the actually measured apparent radii of gyration to those predicted by the power law decrease and assumed

$$\frac{R_{app,\,exp}(c)}{R_{app,power\ law}(c)} \cong \frac{R_g(c)_{scal\ app}}{R_g} \quad (16)$$

The X dependence of these data is shown in Figure 4. The range of variation in the predicted radii in the course of association is large for flexible chains and would be smaller if a rigid-rod structure is assumed. The discrepancy was expected because the upper curve corresponds to noninterpenetrating objects, whereas the scaling approach assumes full interpenetration. Thus, these curves are to be considered as upper and lower limit, and a better description by scaling is expected for flexible chains but for highly branched the upper limit will be more reliable. This behavior was indeed observed with branched samples as examined in a previous paper.[26]

The next question is whether something can be said also about the architecture of these associates. To this end we plotted in Figure 10 $R_g(c)$ against $M_w(c)$ in a double-logarithmic scale. A strong increase of the dimensions is obtained when the rod model is assumed and the data from the virial approach are taken. The same effect, somewhat delayed and shifted to larger molar masses, is observed when the flexible chain model is assumed. The dependencies seem to approach a power law with an exponent $\nu_a = 0.65$, which would correspond to a fractal dimension of $\langle d_{fa}\rangle = 1.54$, where the $\langle ...\rangle$ brackets indicate the ensemble average and the subscript "a" indicates associate. A marked stiffening in the initial process of association (by a factor about 10 for the Kuhn segment length, i.e., $l_K \cong 150$ nm) might be deduced, but this conclusion is not safe because of the uncertainty with the applied virial approach. On the other hand, only the data from the scaling approach result as expected in a straight line through the origin and do not show such stiffening. The whole curve could be nicely fitted by a power law that runs through the origin. The resulting slope is with $\nu_a = 0.548$ almost identical with that obtained for the samples at infinite dilution.[6]

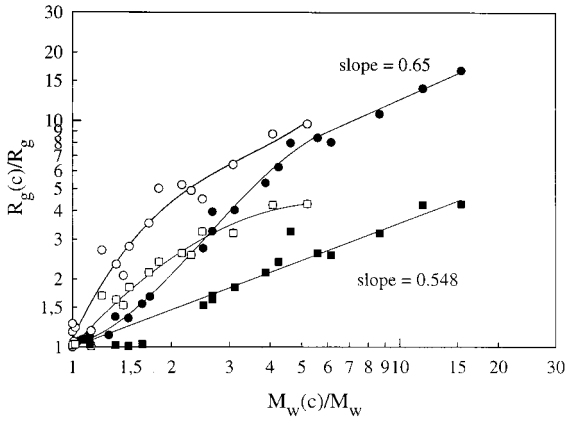

Figure 10. Plot of the normalized true radii of gyration $R_g(c)/R_g$ as a function of the normalized true molar mass assuming interactions among coils (●) and rods (○), respectively. The steep increase of $R_g(c)$ would indicate stiffening of the particles because of lateral association of chains. The asymptotic slope corresponds to an ensemble average fractal dimension $\langle d_f\rangle = 1.54$. The filled circles correspond to the interaction among flexible linear chains the open ones among stiff rods. However, only the scaling approach (eq 16) results in the expected straight line through the origin (filled squares). Its slope corresponds to a fractal dimension of $\langle d_f\rangle = 1.82$. For further details see text.

However, this ν_a exponent will probably not reflect the correct fractal dimension. During association a side-by-side association will take place simultaneously with a growth in length. Because of the side-by-side alignment, a certain additional stiffening of the chain occurs that would increase the exponent. On the other hand, the increase in bundle thickness will lower the exponent, and on the whole, the measured exponent is the result of two counterbalancing effects. The shape of the angular dependent scattering curves give clear indication for a side-by-side alignment and will be analyzed quantitatively in a forthcoming paper.

Dynamic Light Scattering. *Shape of the TCF.* The results at low concentrations were already published in part 1.[6] The TCF shows in that regime common behavior and could be described by only one mode of motion that is related to the apparent mutual diffusion coefficient as described by eq 6. A value of $C = 0.133$ was found (see eq 6), in agreement with theoretical predictions on the basis of Kirkwood's preaverage approximation.[33] At

Table 1. Static Light Scattering Data of the Apparent Molar Mass and Radius of Gyration from a Linters Cellulose in Cd-tren at Various Concentrations[a]

c, g/L	$M_{app}(c)$, g/mol	$R_{g,app}(c)$, nm	$X = A_2M_wc$	$M_w/M_{app}(c)$	$M_w(c)/M_w$	$R_g(c)/R_g$[b]	$M_w(c)/M_w$	$R_g(c)/R_g$[c]
0.000	2.22×10^6	145.0	0.00	1.00	1.00	1.00	1.00	1.00
0.206	1.05×10^6	105.0	0.57	2.12	1.13	1.12	1.01	1.06
0.412	656 000	78.7	1.15	3.38	1.29	1.13	0.97	0.98
0.618	507 000	76.6	1.72	4.37	1.48	1.34	1.14	1.18
0.824	398 000	71.7	2.29	5.57	1.35	1.36	1.00	1.17
1.029	337 000	68.7	2.86	6.59	1.63	1.55	1.02	1.22
1.504	236 000	60.1	4.18	9.39	1.72	1.67	1.00	1.27
2.019	259 000	85.5	5.62	8.57	2.50	2.73	1.43	2.07
2.811	182 000	82.9	7.82	12.22	2.67	3.25	1.36	2.32
3.524	161 000	88.9	9.80	13.79	3.12	4.02	1.49	2.78
4.276	110 000	77.9	11.89	20.24	2.67	3.95	1.23	2.68
5.048	130 400	94.6	14.04	17.03	3.88	5.30	1.71	3.52
6.097	116 500	100.0	16.96	19.05	4.25	6.23	1.83	5.01
7.602	127 600	129.0	21.14	17.40	4.63	7.96	2.49	4.50
8.809	95 600	107.0	24.50	23.22	5.60	8.40	2.15	5.20
10.10	89 100	94.0	28.09	24.90	6.16	8.03	2.30	4.90
12.06	100 900	112.0	83.54	22.00	8.68	10.71	3.09	6.39
13.56	118 388	145.0	37.72	18.75	11.76	13.87	4.08	8.74
15.03	136 813	153.0	41.80	16.23	15.42	16.64	5.21	9.67

[a] For the definition of the apparent quantities see eqs 2 and 3. The molecular parameters at $c = 0$ are $M_w = 2.22 \times 10^6$ g/mol, $R_g = 145$ nm, and $A_2 = 1.25 \times 10^{-3}$ mol mL/g^2 and $A_2M_w = 2.78$ L/g. The data to the right were calculated from the master curves for flexible chains and rigid rods, respectively. [b] Derived with eq 11 for the interaction among flexible chains. [c] Dereived with eq 12 for interactions among stiff rods with axial ratio $p > 100$.

concentrations well above the overlap concentration, however, a second slow motion occurs and gains increasingly influence as c is increased (see Figures 5 and 6).

Fast and Slow Modes of Motion. The TCF could be split into the fast and slow modes by applying an analysis on the basis of the Kohlrausch−Williams−Watts (KWW)[17] approach that uses stretched exponentials to describe the TCF (see Appendix):[18−22]

$$g_1(q,t) = a_f \exp[-(t/\tau_f)^{\beta_f}] + a_s \exp[-(t/\tau_s)^{\beta_s}] \quad (17)$$

Figure 6 shows the concentration dependencies of the diffusion coefficients of these two modes. Note: the decay constant $\Gamma = 1/\tau$ in eq 5 is actually a reciprocal relaxation time that in the KWW approach is represented by the average relaxation times $\langle\tau\rangle_{f,s}$, which are given by the equation

$$\langle\tau\rangle_{f,s} = (\tau_{f,s}/\beta_{f,s})\Gamma(1/\beta_{f,s}) \quad (18)$$

Multiplication of $\langle\tau\rangle_{f,s}$ by q^2 gives $1/D_{app}(q)_{f,s}$. These values have to be extrapolated toward $q^2 = 0$ which gives the mutual diffusion coefficients of the two components. The upper part of Figure 6 shows the concentration dependencies of the two moieties a_f and a_s of the fast (f) and slow (s) motions. With these data the first cumulant could be calculated whose data are shown in the lower part of Figure 6 and are collected in Table 2.

The concentration dependence of the mutual diffusion coefficient D_c is determined by thermodynamic *and* hydrodynamic interactions among the particles. Irreversible thermodynamics shows[34,35]

$$D_c = \frac{kT}{f(c)}\left[\frac{M_w(c)}{RT}\frac{\partial\pi}{\partial c}\right] = D_z\frac{f_0}{f(c)}\frac{M_w(c)}{M_{app}(c)} = D_{self}(c)\frac{M_w(c)}{M_{app}(c)} \quad (19)$$

in which $f(c)$ and f_0 denote the friction coefficients at concentration c and $c = 0$, respectively, and D_z is the z-average translational diffusion coefficient. $D_{self}(c)$ is to be considered as self-diffusion coefficient which may be comparable with the directly measured ones by forced Rayleigh scattering.

Table 2. Diffusion Coefficients of the Fast and Slow Motion (Subscripts f and s) as a Function of Concentration and Scaled Concentration X and Amplitude Factors of These Two Motions

c, g/L	$X = A_2M_wc$	10^8D_f, cm^2/s	a_f	$10^{10}D_s$, cm^2/s	a_s	10^8D_{cum},[a] cm^2/s
0.000	0.00	1.32	1.99		0.00	1.32
0.206	0.57	1.47	1.00		0.00	1.47
0.412	1.15	1.47	1.00		0.00	1.47
0.618	1.72	1.68	1.00		0.00	1.68
0.824	2.29	1.91	1.00		0.00	1.91
1.029	2.86	1.87	1.00		0.00	1.87
1.504	4.18	1.91	1.00		0.00	1.91
2.019	5.62	3.79	0.54	9.69	0.46	2.09
2.811	7.82	5.31	0.51	5.97	0.49	2.74
3.524	9.80	6.46	0.42	3.04	0.58	2.73
4.276	11.89	6.74	0.51	2.26	0.48	3.45
5.048	14.04	7.24	0.40		0.60	
6.097	16.96	7.68	0.43	0.396	0.57	3.30
7.602	21.14	8.58	0.30	0.280	0.70	2.58
8.809	24.50	9.55	0.26	0.278	0.74	2.49
10.10	28.09	10.03	0.25	0.167	0.75	2.51
12.06	83.54	11.26	0.24	0.226	0.76	2.70
13.56	37.72	11.31	0.25	0.015	0.75	2.83
15.03	41.80	11.12				

[a] The cumulant diffusion coefficient was calculated as $D_{cum} = a_fD_f + a_sD_s$.

Equation 18 allows us to split off the influence of the thermodynamic interaction after dividing D_c by the reduced osmotic modulus $M_w(c)/M_{app}(c)$ that was measured by static LS. Equation 18 suggests a writing analogue to eq 7 of[30]

$$\frac{R_h(c)}{R_h} = \frac{f(c)}{f_0} = \frac{D_z}{D_{self}(c)} \quad (20)$$

The equation makes clear that $R_h(c)$ is not the hydrodynamic radius of the cluster but rather a correlation length that describes the range of a hydrodynamic influence and can be considerably larger than the cluster radius, because the friction $f(c)$ depends on the cluster size as well as on the hydrodynamic interaction

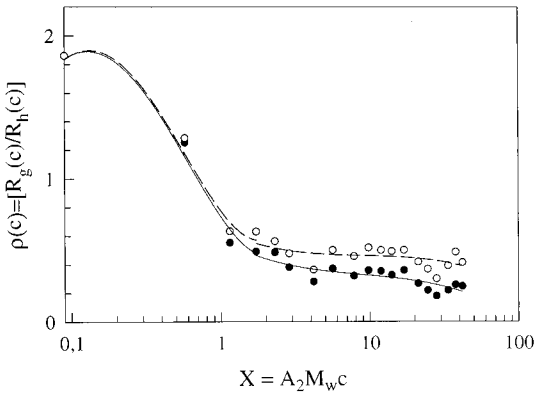

Figure 11. Plot of $R_g(c)/R_h(c)$ as a function of the scaled concentration X. Notation of symbols as in Figure 10.

among the clusters. The latter causes an increase of the viscosity in the neighborhood of the clusters. Figure 6 (right axis) shows the variation of the normalized self-diffusion coefficient in comparison to the behavior of the mutual diffusion coefficient. Two different curves were obtained depending on whether the repulsive interaction between flexible coils or stiff rods were taken. These two curves represent the increase of the hydrodynamic friction with concentration. As was shown in eq 19, the friction can be assumed to be proportional to a correlation length of hydrodynamic influence. In Figure 11 the ratio of $R_g(c)/R_h(c)$ is shown as a function of concentration. One notices that the influence of hydrodynamic interaction exceeds up to 5 times the cluster size. If the radii from the scaling approach are taken (not shown), the ratio becomes with a factor 25 even more pronounced.

Rheological Results. *Zero Shear Viscosity*. Quite normal behavior was observed with a kink point at $c[\eta]_{cr} = 4$ (crossing point of the two limiting lines) and a specific viscosity $\eta_{spec,cr} \cong 10$. Very similar values were found for other linear polymers.[36] Also, the slope of $\mu_\eta = 4.75 \pm 0.09$ corresponds to expectation for linear chains according to which the following relationship should hold

$$\mu_\eta \alpha = 3.5 \tag{21}$$

where α is the Kuhn−Mark−Houwink exponent of the intrinsic viscosity, and the value 3.5 is the experimental exponent for the melt viscosity as a function of molar mass. The Kuhn−Mark−Houwink exponent $\alpha = 0.72 \pm 0.03$ was determined in part 1 of this study. Together with the experimental exponent of μ_η, this gives $(\mu_\eta\alpha)_{exp} = 3.42 \pm 0.16$, in good agreement with the theoretical prediction.[37] Our result deviates from the general relationship published by Morris et al.,[38] who found much lower exponents of $\mu_\eta \approx 3.3$ (see also ref 39).

Shear Dependence. The decrease of the viscosity under shear can be the result of molecular coil deformation and orientation in flow direction, or it can result from disengagement of entangled chains. In any case it is correlated to a certain relaxation time. This behavior agrees with the considerations by Cross,[39,40] who derived the following semiempirical relationship:

$$\frac{\eta - \eta_\infty}{\eta_0 - \eta_\infty} = \frac{1}{1 + [(d\gamma/dt)/(d\gamma/dc)_c]^n} \cong \frac{\eta - \eta_s}{\eta_0 - \eta_s} \tag{22}$$

In this equation η_0 is the zero shear viscosity (Newton behavior) and η_∞ the constant solution viscosity at large shear rates (second Newton niveau). The latter value could not be realized with the available rheometer, but its value is low and equals approximately the solvent viscosity η_s. All curves could be fitted with this Cross equation. The data for the zero shear viscosity the critical shear gradient $d\gamma/dc$ and the exponent n are given in Table 3. A weak increase of this exponent from $n = 0.63$ to 0.77 was observed with an average of $n = 0.74 \pm 0.07$. Similar behavior was found with other linear chain molecules.[41]

Table 3. Zero Shear Rate Viscosities η_0 as a Function f, the Scaled Concentration $c[\eta_0]$, and the Corresponding Critical Shear Rates $(d\gamma/dt)_c = 1/\tau_d$ Determined by a Fit with the Cross Relationship[a]

c, g/L	$c[\eta]$	η_0, Pa·s	η_{spec}	$(d\gamma/dt)_c = 1/\tau_d$, 1/s	n
0.201	0.35	0.00293	0.385		
0.401	0.70	0.00394	0.857		
0.602	1.06	0.0521	1.460		
0.802	1.41	0.0677	2.193		
1.00	1.76	0.0885	3.175		
5.01	8.78	0.596	2.80×10^2	21.1	0.73
7.55	13.19	4.10	1.93×10^3	3.43	0.72
9.04	15.83	10.41	4.91×10^3	1.23	0.63
10.02	17.56	13.01	6.14×10^3	1.86	0.86
12.04	21.10	37.76	1.78×10^4	0.552	0.67
15.01	26.31	109.7	5.18×10^4	0.351	0.77
18.03	31.62	262.3	12.38×10^4	0.195	0.77

[a] The exponent n corresponds to the asymptotic slope. Its average is $n = 0.75 \pm 0.07$. In the dilute regime the viscosity was measured in a capillary viscometer. From 5 g/L onward the rheology showed shear thinning that was measured in a CS Bohlin instrument.

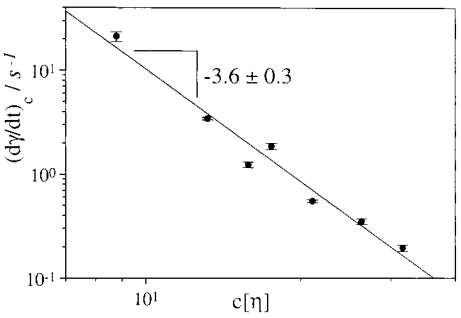

Figure 12. Concentration dependence of the reciprocal relaxation time derived from the Cross approximation $(d\gamma/dc)_c = 1/\tau_d$, where τ_d is the disengagement time for entangled chains.

It was of interest whether the shear thinning of the various concentrations follows a certain self-similar scaling relationship. To prove this, the viscosities were normalized with respect to the zero shear viscosity and the shear rate by the critical shear rate. Figure 8b shows that a master curve is indeed obtained with only a slight change in the slope as was already mentioned. As the next point the concentration dependence of the scaling factors was examined. One notices that the critical shear gradient $(d\gamma/dt)_c$ has the dimension of a reciprocal time. This critical time can be interpreted as a relaxation time τ_d for disengagement of the entangled chains. The concentration dependence of this relaxation time is plotted in Figure 12 in a double-logarithmic scale. An increase of this relaxation time with a power law of 3.6 ± 0.3 is observed. The absolute values of τ_d vary from about 0.05 s at 5 g/L ($c[\eta] = 8.78$) to 5 s at 18 g/L ($c[\eta] = 31.6$).

The strong concentration dependence is unexpected. Doi and Edwards[36] derived under the assumption of

disengagement of entangled chains (without reacting stickers) the following asymptotic relationships:

$$\eta_{spec} \propto (c/c^*)^{\mu_\eta}$$
$$\tau_d \propto (c/c^*)^{\sigma}$$
$$D_s \propto (c/c^*)^{\delta} \quad (23)$$

with

$$\mu_\eta = \frac{3}{3\nu - 1}; \quad \sigma = -\frac{3\nu - 3}{3\nu - 1}; \quad \delta = \frac{\nu - 2}{3\nu - 1} \quad (24)$$

where $\nu = 0.55 \pm 0.01$ is the exponent in the molar mass dependence of the radius of gyration as was measured previously.[6] The values calculated with eq 24 are $\mu_\eta = 4.62$, $\sigma = 2.08$, and $\delta = -2.23$. The much stronger slowing down of the mobility as given by the larger exponent of $\sigma = 3.6 \pm 0.09$ indicates that the disengagement of chains is coupled to reversible association. This causes an additional slowing down. A similar conclusion was drawn also by theory[42,43] based on the tube model, according to which the reptating chain is slowed by a factor that depends on the probability of closed stickers. This probability is a fairly complex function of the concentration. Experimentally this slowing down could be described by a power law $\tau_{da}/\tau_d \cong c^{-1.5}$. No power law behavior was found for the self-diffusion coefficients. This may be a result that the measured self-diffusion is not solely caused by disengagement but also by translational motion of clusters. This in turn gives indications that the tube model with its strong restrictions for motions is not a fully satisfactory approach.

Concluding Remarks

Three observations demonstrate the onset of association when the concentration was increased beyond the overlap concentration. These are (i) a strong angular dependence at small scattering angles, (ii) an uncommon concentration dependence of the osmotic modulus in static light scattering, and (iii) the appearance of a slow motion in dynamic light scattering. An attempt was made to quantify the effects and to determine the size of associated clusters. The approach was based on the assumption that the interaction among nonassociated macromolecules and associated clusters is not significantly different. This assumption is strictly correct for hard spheres but requires further studies by new experimental techniques or by computer simulations. Several counteracting processes are effective. The one is the concentration dependence of the probability of forming a bond between stickers, and the other is the effect of increasing molar mass of the particles. The reported data may be overestimations or underestimations, but the general trend will not change significantly. The association behavior is not a specialty of cellulose in the metal-based solvent. Similar effects were also obtained and evaluated with branched macromolecules.

Less definite conclusions could be drawn on the increase of the radii of gyration while association proceeds. Two approaches have been applied. The virial approach may be considered as an upper limit and the scaling approach as a lower limit. Branched chains are expected to be closer to the upper limit, but for deeply interpenetrating chains the lower limit may be more reliable.

The association process has no detectable effect on rheological *behavior*. The zero shear viscosity resembles that of common nonassociating linear chains, and the shear dependence can be scaled by the Cross approximation in the same manner. The insensitivity rheology to large associates results from the fact that in light scattering measurements the *z*-average of particle sizes is observed while in rheology the average is close to the number-average. Therefore, light scattering is sensitive to large particles, i.e., clusters of chains, while rheology mainly probes small sizes corresponding to nonassociated chains.

However, a quantitative evaluation of the concentration dependence for the disengagement relaxation time and the slow diffusion coefficient gave clear evidence for reversible association processes in addition to common disengagement of entangled chains and causes an additional slowing down.

The driving force to association is not known but in the present case is very likely based on hydrogen bonding and chain stiffness that entropically may enhance the probability of association. No indication for a liquid crystalline phase separation was observed. The applied concentration range was much lower than required by theory. An estimation on the basis of the Kuhn segment length gives $c_{LC} \cong 24\%$ for the chains in dilute solution; a corresponding estimation for the aggregates with a probably much larger Kuhn segment length was not possible,[21] because the number of laterally aggregated structures is not known.

One question remained unresolved. The stiff cellulose chains surprisingly obey the interactions among rigid rods, but the investigated chain consisted already of 300 Kuhn segments and had to be considered as being close to Gaussian behavior.

Acknowledgment. This work was done within a scheme of research on cellulose and cellulose derivatives that was kindly supported by the Deutsche Forschungsgemeinschaft. We also thank Professor Peter Klüfers and co-workers, Institute of Inorganic Chemistry, University of Munich, for providing us with the receipt for preparation the Cd-tren solution and for fruitful hints and discussions.

Appendix. Comments to Evaluation Procedures of Time Correlation Functions

The cumulant fit and CONTIN inversion procedures are most convenient in practical application, because the corresponding programs are online available on the ALV 5000 autocorrelator (ALV5000.exe). The unsatisfactory cumulant fit for multirelaxation processes is based on the mathematics that reacts insensitively when more than one relaxation process is effective. The CONTIN program[16] appears especially attractive as it directly shows the distribution of the relaxation spectrum, which can be mono-, bi-, or multimodal. However, it remains essential to recall that the CONTIN inversion is a mathematically "ill-posed" inversion program. This is to say, the Laplace transformation of relaxation processes into TCFs of dynamic light scattering is uniquely defined, but not the inverse Laplace transformation from the TCF into the relaxation spectrum. A large number of very different relaxation spectra $h(\tau)$ can be the result which equally well describes the TCF. Most of these have no physical relevance and can be excluded, e.g., by the constraint that $h(\tau)$ should never

take negative values. Further reduction of physically meaningless solutions are gained by smoothing the original TCF. This was done by Provencher[16] by introducing a regularization parameter by which the fluctuations due to experimental error are locally suppressed. In most cases a constant value is assumed in the CONTIN program that however can be varied manually when larger errors than usually obtained are registered.

Unfortunately, the appropriate choice of the regularization parameter causes problems. It appears almost impossible to judge correctly whether the fluctuations are due to the noise or rather due to a further well-separated peak in the relaxation spectrum. The problem becomes noticeable when for physical reasons three processes should be observed. In a certain angular region (say 75°−105°) consistently such three modes are found. However, at smaller angles suddenly one of the three peaks splits off into two new ones, which cannot be related to the other ones at larger angles. Of course, this splitting can be suppressed by manually increasing the regularization parameter. Honerkamp and Weese[18,19] partially removed this disagreeable inconsistency. They first estimated the experimental error from the experimental TCF curve on the basis of a special error model, and this average error is then used to define an optimum regularization value.

We checked this procedure extensively in a preceding paper[20] with the following result: The derived relaxation peaks in the spectrum were now further characterized by shaded areas, if unreliable results were obtained. On the other hand, the occurrence of 4−5 additional peaks between two widely separated main processes (4−6 decades in time) could not be avoided, and in addition the number of these peaks varied from one scattering angle to another. Again, this number can be made independent of the angle by manually changing the regularization parameters. This procedure turned out to be very time-consuming and remained unsatisfactory because of the arbitrariness.

Such mathematical instabilities do not exist when a curve is *fitted* with well-known Laplace transforms of relaxation processes. Now the data from the whole curve are used simultaneously. Stable results are obtained for systems up to three modes of motion. The required program was developed by R. Dolega in our group. A first idea was given by Kohlrausch[17a] 150 years ago and was taken up again by Williams and Watts[17b] and applied to dielectric relaxation processes. Finally, Patterson et al.[17c,d] introduced this technique to interpret dynamic light scattering time correlation functions. The latter also pointed out some defaults of the stretched exponential.

All these fit attempts were probably made solely on pragmatic grounds. There exist, however, two theoretical observations which support the physical basis of the stretched exponential. The one was given by Akcasu et al.,[21] who showed that at large delay times the TCFs asymptotically approach stretched exponentials with exponents $\beta = {}^1/_2$ for Rouse and $\beta = {}^1/_3$ for Zimm relaxation processes. The other more generalized analysis was presented by Ngai,[22] who gave convincing arguments that such exponentials are indicative for *cooperative* relaxation processes.

References and Notes

(1) Fengel, D.; Wegener; G. *Wood−Chemistry, Ultrastructure, Reactions*; de Gruyter: Berlin, 1989.
(2) Klemm, D.; Philipp, B.; Heinze, T. J.; Heinze, U.; Wagenknecht, W. *Comprehensive Cellulose Chemistry*; Wiley: Weinheim, 1998; Vol. 1.
(3) Schulz, L.; Seger, B.; Burchard, W. *Macromol. Chem. Phys.*, submitted.
(4) Klaassen, M.; Klüfers, P. *Z. Anorg. Allg. Chem.* **1993**, *619*, 661.
(5) (a) Burger, J.; Kettenbach, G.; Klüfers, P. *Macromol. Symp.* **1995**, *99*, 113. (b) Kettenbach, G.; Klüfers, P.; Mayer, P. *Macromol. Symp.* **1997**, *120*, 291.
(6) Saalwächter, K.; Burchard, W.; Klüfers, P.; Kettenbach, G.; Mayer, P.; Klemm, D.; Dugarmaa, S. *Macromolecules* **2000**, *33*, 4094.
(7) Burchard, W.; Habermann, N.; Klüfers, P.; Seger, B.; Wilhelm, U. *Angew. Chem., Int. Ed. Engl.* **1994**, *33*, 884.
(8) De Gennes, P.-G. *Scaling Concepts in Polymer Physics*; Cornell University Press: Ithaca, NY, 1979.
(9) Freed, K. F. *Renormalization Group Theory of Macromolecules*; Wiley: New York, 1987.
(10) (a) Coviello, T.; Kajiwara, K.; Burchard, W.; Crescenzi, V. *Macromolecules* **1986**, *19*, 2826. Dentini, M.; Coviello, T.; Burchard, W.; Crescenzi, V. *Macromolecules* **1988**, *21*, 3320. (c) Denkinger, P.; Burchard, W.; Kunz, M. *J. Phys. Chem.* **1989**, *93*, 1428.
(11) Burchard, W. *Macromol. Symp.* **1990**, *39*, 179.
(12) Otha, T.; Oono, Y. *Phys. Lett.* **1983**,*79*, 839.
(13) Cotter, N. A.; Martire, D. C. *J. Chem. Phys.* **1970**, *52*, 1909.
(14) Berne, B. J.; Pecora, R. *Dynamic Light Scattering;* Wiley: New York, 1976.
(15) Burchard, W.; Schmidt, M.; Stockmayer, W. H. *Macromolecules* **1989**, *13*, 580, 1265.
(16) Provencher, S. W. *Comput. Phys. Commun.* **1982**, *27*, 213, 229.
(17) (a) Kohlrausch, R. *Pogg. Ann. Phys.* Chem. **1854**, *91*, 179; **1863**, *119*, 337. (b) Williams, G.; Watts, D. C. *Trans. Faraday Soc.* **1971**, *66*, 80. (c) Lindsey, C. P.; Patterson, G. D. *J. Chem. Phys.* **1980**, *73*, 3348. (d) Patterson, G. D. *Adv. Polym. Sci.* **1983**, *48*, 148.
(18) (a) Honerkamp, J.; Weese, J. *Continuum Mech. Thermodyn.* **1990**, *2*, 17. (b) Honerkamp, J.; Maier, D.; Weese, J. *J. Chem. Phys.* **1993**, *98*, 2.
(19) Weese, J. *Comput. Phys. Commun.* **1993**, *77*, 429.
(20) Coviello, T.; Burchard, W.; Geissler, E.; Maier, D. *Macromolecules* **1997**, *30*, 2008.
(21) Akcasu, A. Z.; Benmouna, M.; Han, C. C. *Polymer* **1980**, *21*, 866.
(22) Ngai, K. L. In Blumen, A., Ed.; *Disorder Effects on Relaxation Processes;* Springer-Verlag: Berlin, 1994; Chapter 4, pp 81−150.
(23) (a) McQuarrie, D. A. *Statistical Mechanics*; Harper & Row: New York, 1976; p 252. (b) Friedman, H. L. *A Course in Statistical Mechanics*; Prentice-Hall: Englewood Cliffs, NJ, 1985.
(24) Des Cloizeaux, J. *J. Phys. (Paris)* **1975**, *36*, 281.
(25) Carnahan, N. F.; Starling, K. E. *J. Chem. Phys.* **1969**, *51*, 635.
(26) (a) Burchard, W. *Adv. Polym. Sci.* **1999**, *143*, 181. (b) Galinsky, G.; Burchard, W. *Macromolecules* **1996**, *29*, 1498. (c) Aberle, T.; Burchard, W. *Starch* **1997**, *49*, 215. (d) Ioan, C. E.; Aberle, T.; Burchard, W. *Macromolecules* **1999**, *32*.
(27) Ioan, C. E.; Aberle, T.; Burchard, W. *Macromolecules* **2001**, *34*, 326.
(28) Jinbo, Y; Sato, T.; Teramoto, A. *Macromolecules* **1994**, *27*, 6080.
(29) Sato, T.; Jinbo, Y.; Teramoto, A. *Polymer* **1995**, *27*, 384.
(30) Tanaka, F.; Stockmayer, W. H. *Macromolecules* **1994**, *27*, 3943.
(31) Ishida, M.; Tanaka, F. *Macromolecules* **1997**, *30*, 3900.
(32) Semenov, A. N.; Rubinstein, M. *Macromolecules* **1998**, *31*, 1373.
(33) Kirkwood, J. G.; Riseman, J. *J. Chem. Phys.* **1948**, *16*, 565.
(34) De Groot, S. R. *Thermodynamik Irreversibler Prozesse;* Biblographisches Institut: Mannheim, 1960.
(35) Yamakawa, H. *Modern Theory of Polymer Solutions*; Harper & Row: New York, 1971.
(36) Ioan, C. E.; Aberle, T.; Burchard, W. *Macromolecules* **2001**, *34*, 326.
(37) Doi, M.; Edwards, S. F. *The Theory of Polymer Dynamics*; Clarendon Press: Oxford, 1986.
(38) Morris, E. R.; Cutler, A. N.; Ross-Murphy, S. B.; Rees, D. A.; Price, J. *Carbohydr. Polym.* **1981**, *1*, 5.
(39) Lapasin, R.; Pricl, S. *Rheology of Industrial Polysaccharides*; Blackie Academic & Professional: London, 1995.

(40) Cross, M. M. *J. Colloid Sci.* **1965**, *20*, 417.
(41) Morris, E. R. In *Gums and Stabilizers in the Food Industry. 2. Applications of Hydrocolloids;* Phillips, G. O., Wodlock, D. J., Williams, P. A., Eds.; Pergamon Press: London, 1984; pp 57−78.
(42) Gonzales, A. E. *Polymer* **1983**, *24*, 77; **1984**, *25*, 1461.
(43) Leibler, L.; Rubinstein, M.; Colby, R. H. *Macromolecules* **1991**, *24*, 4701.

MA0016073